Electronic Supplementary Material (ESI) for Journal of Materials Chemistry C.

An ultra-high quantum yield Tb-MOF with phenolic hydroxyl as the recognition group for highly selective and sensitive detection of Fe^{3+}

Yuming Zhao,[a] Xu Zhai,[a] Lei Shao,[a] Linlin Li,[a] Yunling Liu,[c] Xuemin Zhang,[a] Jinhui Liu,*[b] Faobao Meng,*[a] and Yu Fu*[a]

[a]Department of Chemistry, College of Sciences, Northeastern University, Shenyang 110819, P. R. China.*E-mail: fuyu@mail.neu.edu.cn.

*E-mail: mengfb@mail.neu.edu.cn.

[b]Henan Province Industrial Technology Research Institute of Resources and Materials, Zhengzhou University, Zhengzhou 450001, P. R. China.

*E-mail: liujinhui@zzu.edu.cn.

[c]State Key Laboratory of Inorganic Synthesis and Preparative Chemistry, College of Chemistry, Jilin University, Changchun 130012, P. R.China.

Materials. Terbium(III) acetate hexahydrate [$Tb(OAc)_3 \cdot 6H_2O$], 2-hydroxyterephthalic acid ($H_2BDC\text{-}OH$) were purchased from Energy Chemical (Shanghai, China). N,N-dimethylformamide (DMF), ethanol, methanol, acetonitrile (CH_3CN), N, N-dimethylacetamide (DMAC) were purchased from Sinopharm Chemical Reagent Co., Ltd. Ferric chloride hexahydrate ($FeCl_3 \cdot 6H_2O$), Zinc acetate [$Zn(OAc)_2$], potassium chloride (KCl), sodium chloride (NaCl), Nickel chloride hexahydrate ($NiCl_2 \cdot 6H_2O$), Manganese chloride tetrahydrate ($MnCl_2 \cdot 4H_2O$), Cobalt chloride hexahydrate ($CoCl_2 \cdot 6H_2O$), Magnesium acetate tetrahydrate [$Mg(OAc)_2 \cdot 4H_2O$], Chromium chloride hexahydrate ($CrCl_3 \cdot 6H_2O$) were purchased from Sinopharm Chemical Reagent Co., Ltd. Pure water was purchased from Shenyang Wahaha Group Co., Ltd. All chemicals used in this study were of analytical grade and used without further purification.

Characterization. The crystalline structures of the samples were determined using X-ray diffraction (XRD, Shimadzu XRD-6000) equipped with Cu Kα radiation (λ = 1.5406 Å) in the 2θ range of 5°-50° at room temperature. A thermostability test was performed by thermal gravimetric analyzer (TGA-2050, TA Instruments) under N_2 from room temperature to 1000 ^oC with a heating rate of 10 ^oC min^{-1}. The micro-scale morphology images coupled with energy dispersive X-ray spectroscopy (EDX) were obtained by field-emission scanning electron microscopy (FE-SEM, Hitachi SU8010) at primary electron energy of 15 kV equipped with an EDX instrument. The optical photographs were taken by a positive fluorescence microscope (Olympus, BX53M). The organic groups of MOF were characterized by Fourier transform infrared spectroscopy (FT-IR, Bruker VERTEX 70) with KBr pellets. The compositions of the materials were analyzed through quantitative X-ray photoelectron spectroscopy (XPS, Thermo Scientific Escalab 250Xi). The absorption spectra at 200-800 nm were measured with an optical spectrometer (Ocean Optics, Maya 2000Pro). A fluorescence spectrophotometer (FluoroMax-4, HORIBA) equipped with a 150 W xenon lamp as the excitation source was used to collect the fluorescence spectra of the Tb-MOF samples. The Density functional theory (DFT) calculations were performed using Gaussian16 at thePBE0/6-311g(d) level with the D3(BJ) empirical dispersion correction.

Tab. S1 Crystal data and structure refinement for Tb-MOF.

Empirical formula	$C_{36}H_{39}N_4O_{19}Tb_2$
Formula weight	1149.55
Temperature	193 K
Wavelength	1.34139 Å
Crystal system	Triclinic
Space group	P-1
Unit cell dimensions	a = 10.4852(5) Å
	b = 11.1327(5) Å
	c = 12.5441(6) Å
	α= 103.880(2)°
	β= 109.922(2)°
	γ= 96.693(2)°
Volume	1304.51(11) $Å^3$
Z	1
Density (calculated)	1.463 g/m^3
Absorption coefficient	14.322 mm^{-1}
F(000)	565.0
Crystal size	0.120 x 0.1 x 0.1 mm^3
Theta range for data collection	3.417 to 63.380°
Index ranges	-13<=h<=13
	-14<=k<=14
	-15<=l<=16
Reflections collected	17647
Independent reflections	6178 [R(int) = 0.0447]
Completeness to theta=63.412°	95.4 %
Refinement method	Full-matrix least-squares on F^2
Data / restraints / parameters	6178 / 38 / 352
Goodness-of-fit on F2	1.057
Final R indices [I>2sigma(I)]	R1 = 0.0278, wR2 = 0.0761
R indices (all data)	R1 = 0.0290, wR2 = 0.0768
Extinction coefficient	n/a
Largest diff. peak and hole	0.425 and -0.512 $e.Å^{-3}$

Tab. S2 Selected bond lengths (Å) for Tb-MOF.

Tb(1)O(4)	2.310(3)
Tb(1)-O(1)	2.367(3)
Tb(1)-O(8)	2.418(3)
Tb(1)-O(9)	2.507(2)
Tb(1)-O(10)	2.419(3)
Tb(1)-O(7A)	2.43(1)
Tb(1)-O(4)	2.827(2)
Tb(1)-O(5)	2.385(2)
Tb(1)-O(2)	2.353(2)

Tab. S3 Selected bond angles (°) for Tb-MOF.

O(4)-Tb(1)-O(1)	76.50(9)
O(4)-Tb(1)-O(8)	144.79(8)
O(4)-Tb(1)-O(9)	131.63(8)
O(4)-Tb(1)-O1(0)	84.6(1)
O(4)-Tb(1)-O7(A)	79.7(3)
O(4)-Tb(1)-O(4)	74.90(7)
O(4)-Tb(1)-O(5)	123.98(8)
O(4)-Tb(1)-O(2)	77.59(9)
O(1)-Tb-(1)-O(8)	138.62(9)
O(1)-Tb(1)-O(9)	71.82(9)
O(1)-Tb(1)-O (10)	74.9(1)
O(1)-Tb(1)-O(7A)	142.4(3)
O(1)-Tb(1)-O(4)	66.00(8)
O(1)-Tb(1)-O(5)	77.89(8)
O(1)-Tb(1)-O(2)	129.99(9)
O(8)-Tb(1)-O(9)	75.70(9)
O(8)-Tb(1)-O(10)	104.6(1)
O(8)-Tb(1)-O(7A)	70.7(3)
O(8)-Tb(1)-O(4)	112.78(8)
O(8)-Tb(1)-O(5)	73.69(8)
O(8)-Tb(1)-O(2)	75.10(9)
O(9)-Tb(1)-O(10)	52.6(1)
O(9)-Tb(1)-O(7A)	104.7(3)
O(9)-Tb(1)-O(4)	121.09(8)
O(9)-Tb(1)-O(5)	83.76(8)
O(9)-Tb(1)-O(2)	150.18(9)
O(10)-Tb(1)-O(7A)	74.2(3)
O(10)-Tb(1)-O(4)	138.92(9)
O(10)-Tb(1)-O(5)	133.8(1)
O(10)-Tb(1)-O(2)	143.0(1)
O(7A)-Tb(1)-O(4)	133.8(3)
O(7A)-Tb(1)-O(5)	139.7(3)
O(7A)-Tb(1)-O(2)	70.9(3)
O(4)-Tb(1)-O(5)	49.18(7)
O(4)-Tb(1)-O(2)	66.29(8)
O(5)-Tb(1)-O(2)	82.37(8)

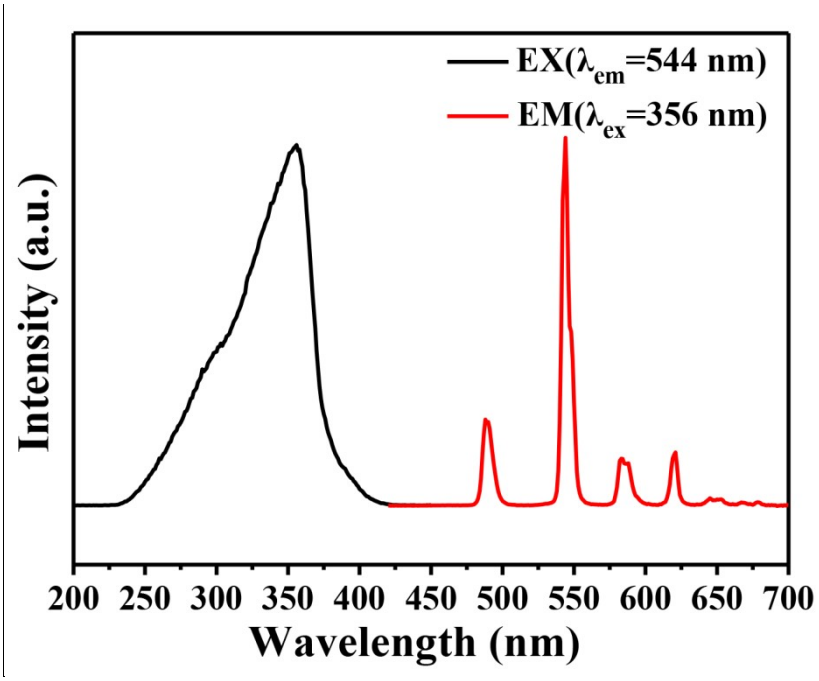

Fig. S1 Solid state excitation (blank line) and emission spectra (red line) of Tb-MOF (2- hydroxyterephthalic acid as the ligand) at room temperature.

Tab. S4 The singlet and triplet energy levels of H_2BDC-OH ligand.

Multiplicity	Excited state	Excitation energy
T	1	3.0733 eV
S	1	4.2095 eV

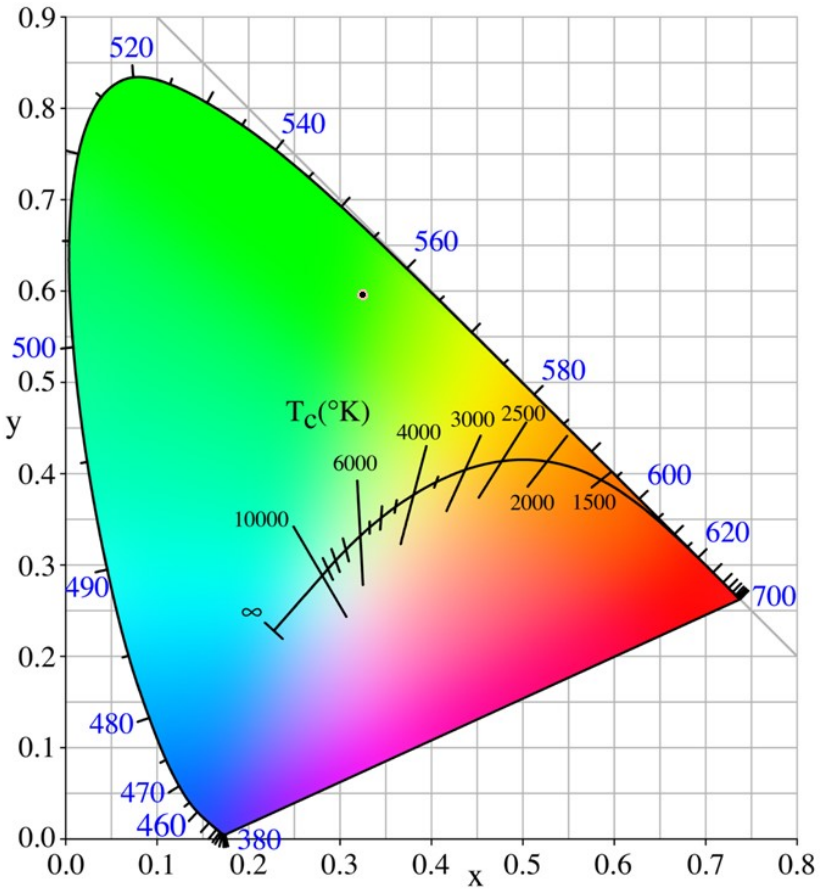

Fig. S2 The corresponding CIE chromaticity diagrams of Tb-MOF.

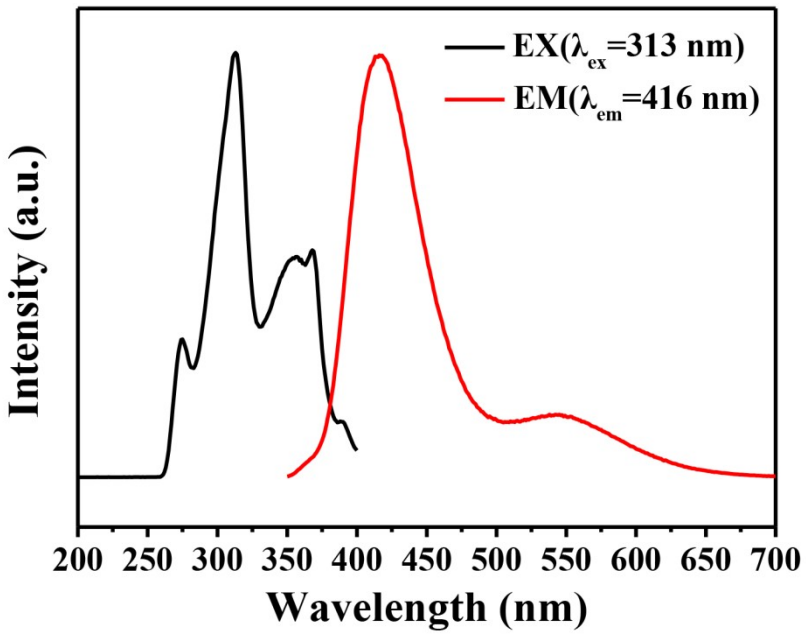

Fig. S3 Solid state excitation (blank line) and emission (red line) spectra of Tb-MOF-1 (2,5-dihydroxy terephthalic acid as the ligand) at room temperature. The results find that Tb-MOF-1 does not exhibit characteristic emission peaks of Tb^{3+} under the optimal excitation wavelength of 313 nm, but shows a strong ligand emission peak at 416 nm.

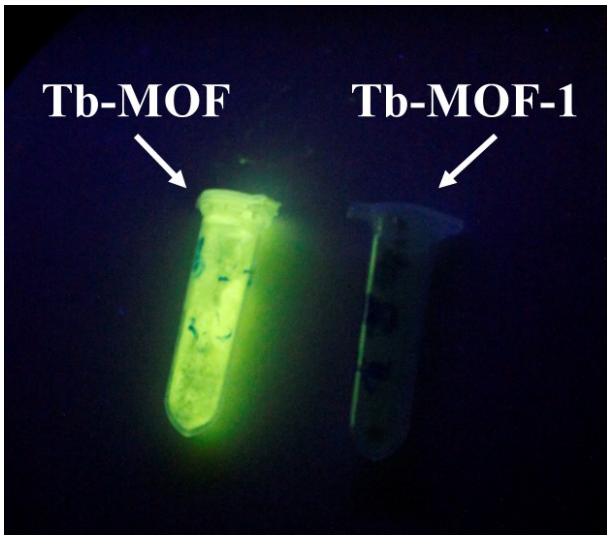

Fig. S4 The corresponding luminescence picture of Tb-MOF and Tb-MOF-1 under UV light irradiation of 365 nm.

Tab. S5 The singlet and triplet energy levels of H_4dobdc ligand.

Multiplicity	Excited state	Excitation energy
T	1	2.6015 eV
S	1	3.7101 eV

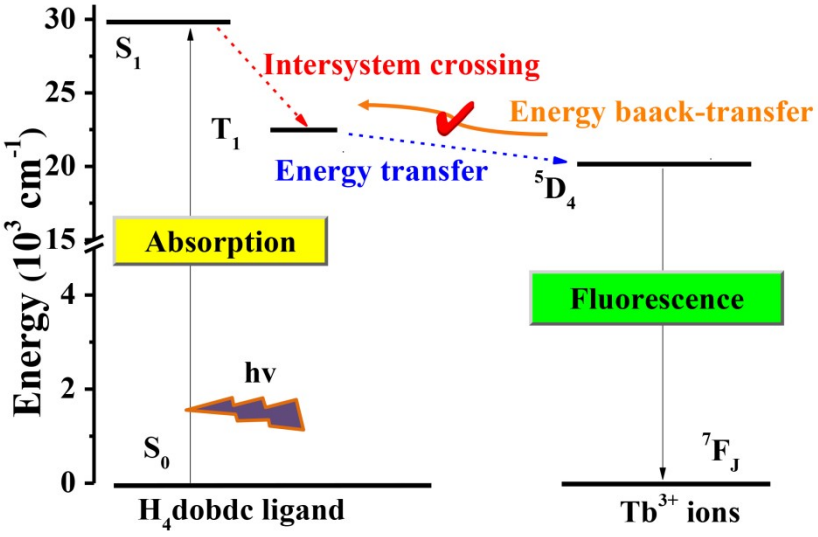

Fig. S5 Schematic diagram of energy absorption, transfer and emission process of Tb-MOF-1 (S_0=ground state, S_1=the first excited singlet state, T_1=the first excited triplet state).

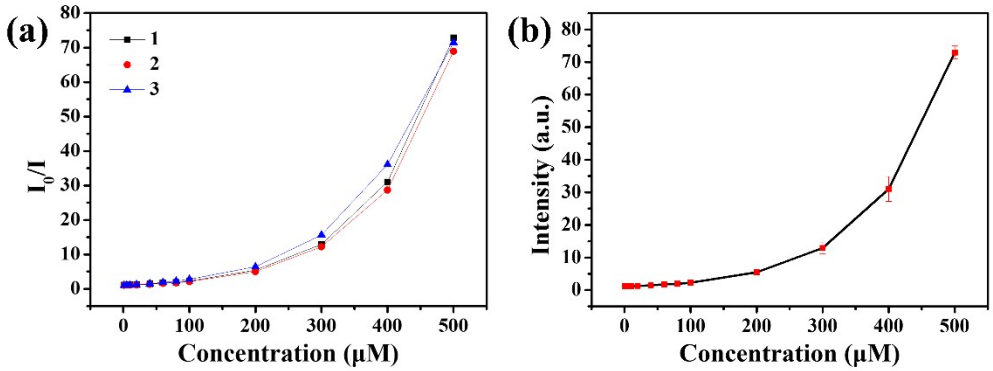

Fig. S6 (a) The relationship between fluorescence intensity (I_0/I) and concentration of Fe^{3+} of the three times, (b) The relationship between fluorescence intensity (I_0/I) and concentration of Fe^{3+} with error bars.

Tab. S6 The K_{sv} comparison between various MOF materials for Fe^{3+}.

	K_{sv}	Ref
EuL^1_3	4.1×10^3	[1]
$(Me_2NH_2)[Tb(OBA)_2](Hatz)(H_2O)_{1.5}$	3.4×10^4	[2]
Eu@MIL-53-COOH	5.12×10^3	[3]
$Eu(L^2)(BPDC)_{1/2}(NO_3)$	5.16×10^4	[4]
$[(CH_3)_2NH_2][Ca(Me_2tcpbH)(H_2O)$	1.18×10^5	[5]
Tb-MOF	1.63×10^5	This work

L^1=4’-(4carboxyphenyl)-2,2’:6’,2”-terpyridine

L^2= 2,5-di(pyridin-4-yl)terephthalic acid

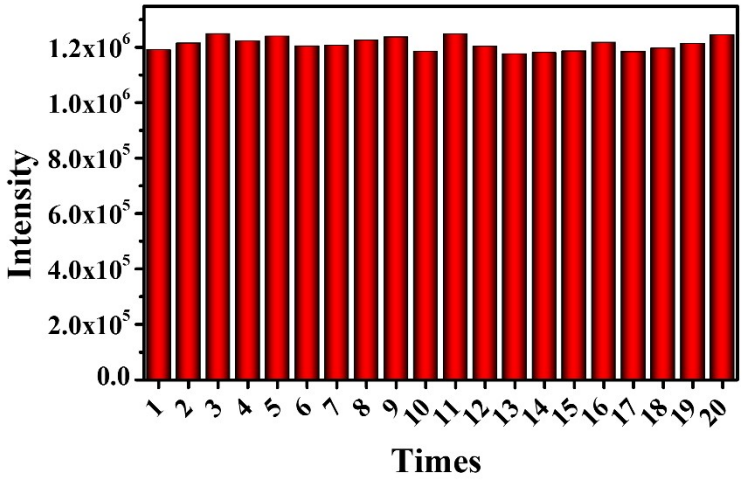

Fig. S7 The fluorescence intensity (λem=544 nm) of Tb-MOF (0.1 mg mL-1) for twenty times.

The standard deviation of blanks for twenty times is calculated to be 0.019151. The *k* is the slope of Stern-Volmer equation, here is K_{sv}, which is 0.16257 μM^{-1}. Therefore, the detection limit of Tb-MOF for Fe^{3+} is calculated to be 0.35 μM according to the 3σ/k formula.

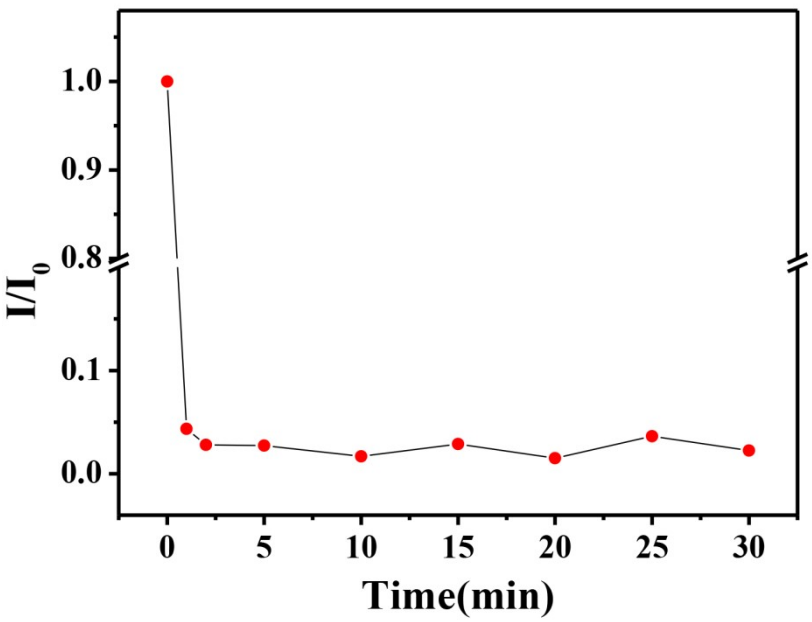

Fig. S8 The fluorescence quenching efficiency (I/I_0) of Tb-MOF (0.1 mg mL^{-1}) changes with time in the presence of Fe^{3+} (0.5 mM).

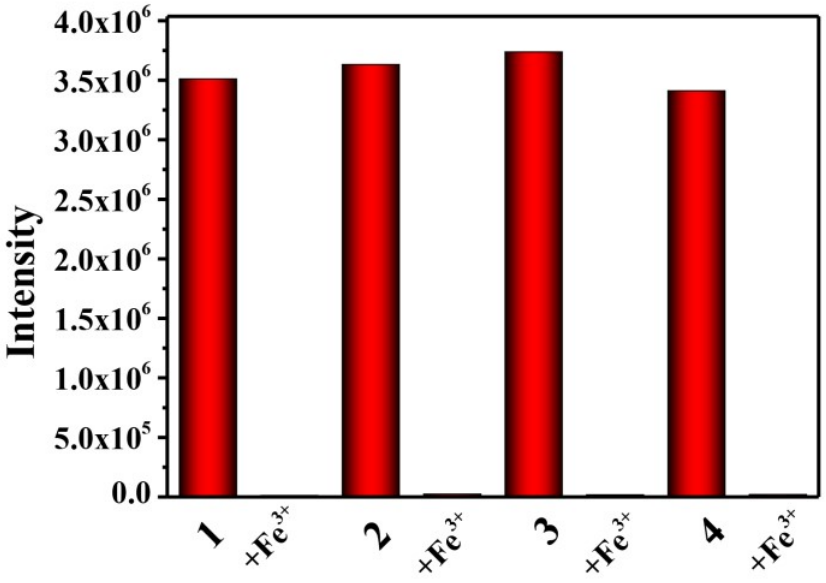

Fig. S9 The reproducibility for Tb-MOF in detecting Fe^{3+}.

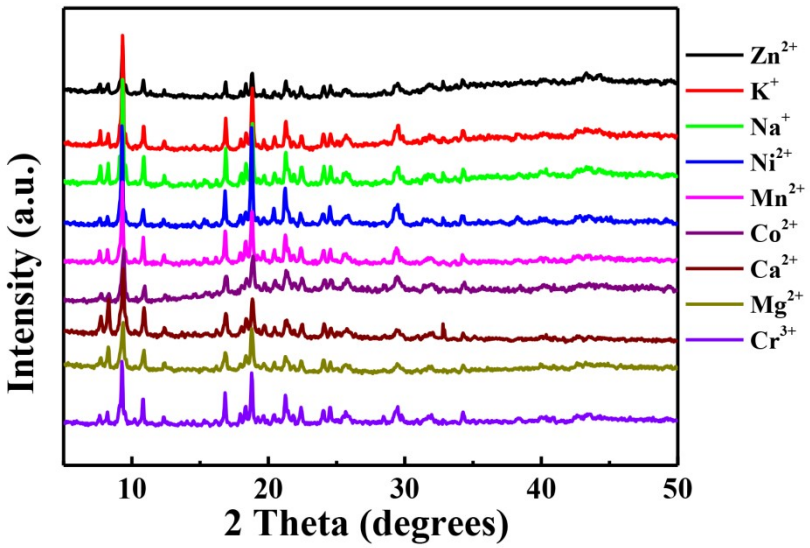

Figue S10 XRD patterns of Tb-MOF DMF solution after adding different metal ions. The XRD patterns of Tb-MOF after adding different metal ions are consistent with the original synthesized sample, indicating that the structure of Tb-MOF does not change, thus proving that fluorescence quenching is not caused by the collapse of MOF skeleton.

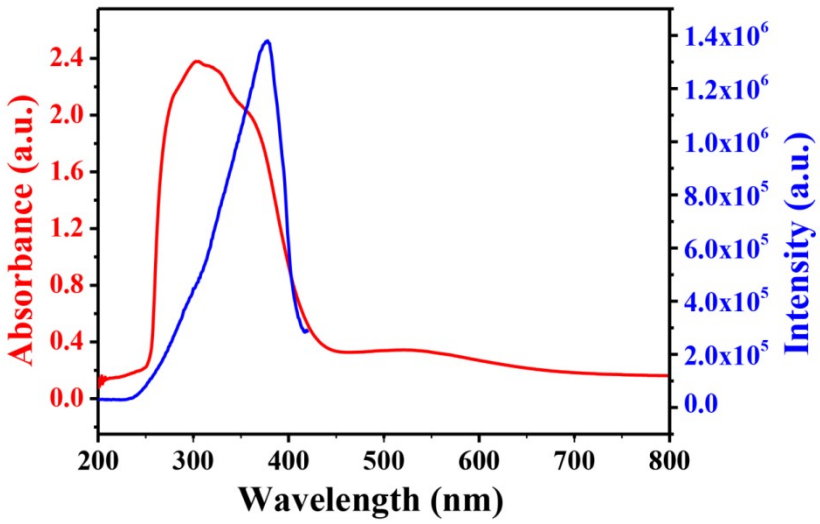

Fig. S11 The absorption spectrum of Fe^{3+} (1 mM) and the excitation spectrum of H_2BDC-OH powder.

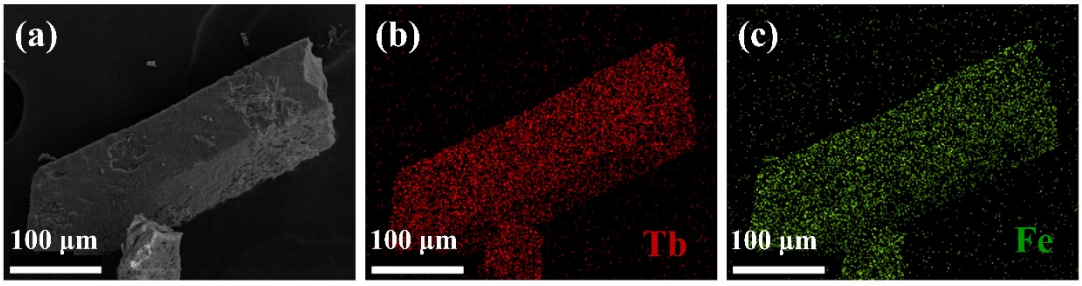

Fig. S12 The SEM and energy-dispersive X-ray (EDX) elemental mapping images of Tb-MOF.

Reference

1. M. Zheng, H. Tan, Z. Xie, L. Zhang, X. Jing and Z. Sun, *ACS Appl. Mater. Interfaces*, 2013, **5**, 1078-1083.
2. D.-M. Chen, N.-N. Zhang, C.-S. Liu and M. Du, *J. Mater. Chem. C*, 2017, **5**, 2311-2317.
3. Y. Zhou, H.-H. Chen and B. Yan, *J. Mater. Chem. A*, 2014, **2**, 13691-13697.
4. W. T. Koo, J. S. Jang, S. J. Choi, H. J. Cho and I. D. Kim, *ACS Appl. Mater. Interfaces*, 2017, **9**, 18069-18077.
5. Z.-F. Wu, Z.-H. Fu, E. Velasco, K. Xing, H. Wang, G.-D. Zou, X.-Y. Huang and J. Li, *J. Mater. Chem. C*, 2020, **8**, 16784-16789.